

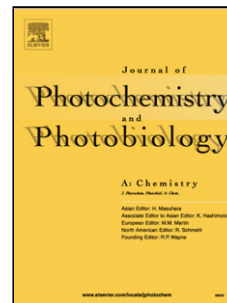
This is the Post-print version of the following article: *R. Camposeco, S. Castillo, Isidro Mejía-Centeno, J. Navarrete, N. Nava, V. Rodríguez-González, Synthesis of protonated titanate nanotubes tailored by the washing step: Effect upon acid properties and photocatalytic activity, Journal of Photochemistry and Photobiology A: Chemistry, Volume 341, 2017, Pages 87-96*, which has been published in final form at: <https://doi.org/10.1016/j.jphotochem.2017.03.012>

© 2017. This manuscript version is made available under the CC-BY-NC-ND 4.0 license <http://creativecommons.org/licenses/by-nc-nd/4.0/>

## Accepted Manuscript

Title: Synthesis of protonated titanate nanotubes tailored by the washing step: Effect upon the acid properties and photocatalytic activity

Authors: R. Camposeco, S. Castillo, Isidro Mejía-Centeno, J. Navarrete, N. Nava, V. Rodríguez-González



PII: S1010-6030(16)30823-1  
DOI: <http://dx.doi.org/doi:10.1016/j.jphotochem.2017.03.012>  
Reference: JPC 10563

To appear in: *Journal of Photochemistry and Photobiology A: Chemistry*

Received date: 27-9-2016  
Revised date: 20-1-2017  
Accepted date: 9-3-2017

Please cite this article as: R.Camposeco, S.Castillo, Isidro Mejía-Centeno, J.Navarrete, N.Nava, V.Rodríguez-González, Synthesis of protonated titanate nanotubes tailored by the washing step: Effect upon the acid properties and photocatalytic activity, *Journal of Photochemistry and Photobiology A: Chemistry*<http://dx.doi.org/10.1016/j.jphotochem.2017.03.012>

This is a PDF file of an unedited manuscript that has been accepted for publication. As a service to our customers we are providing this early version of the manuscript. The manuscript will undergo copyediting, typesetting, and review of the resulting proof before it is published in its final form. Please note that during the production process errors may be discovered which could affect the content, and all legal disclaimers that apply to the journal pertain.

# **Synthesis of protonated titanate nanotubes tailored by the washing step: Effect upon the acid properties and photocatalytic activity**

R. Camposeco<sup>1\*</sup>, S. Castillo<sup>2</sup>, Isidro Mejía-Centeno<sup>3</sup>, J. Navarrete<sup>3</sup>, N. Nava<sup>3</sup> and V. Rodríguez-González<sup>1</sup>

<sup>1</sup>*Instituto Potosino de Investigación Científica y Tecnológica, División de Materiales Avanzados, 78216, San Luis Potosí, S.L.P.; México*

<sup>2</sup>*Dirección de Tecnología del Producto, Instituto Mexicano del Petróleo, 07730, México, D.F.; México*

<sup>3</sup>*Dirección de Investigación en Transformación de Hidrocarburos, Instituto Mexicano del Petróleo, 07730, México, D.F.; México*

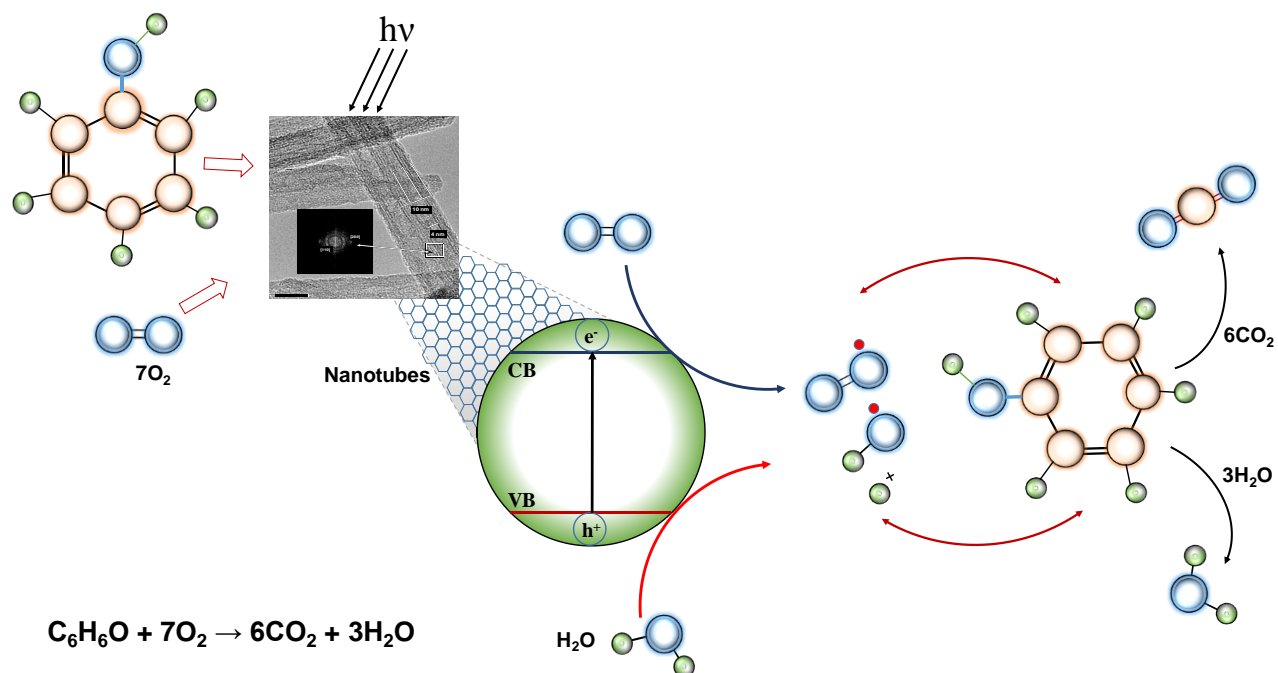
\*Corresponding author.

*Tel:* + (52) 55 9175 8216;

*Fax:* + (52) 55 9175 9699

*E-mail address:* [roberto.camposeco@ipicyt.edu.mx](mailto:roberto.camposeco@ipicyt.edu.mx)

## Graphical abstract



## Highlights

- Three different acid agents were used to prepare nanotubes of  $TiO_2$
- $HCl$ ,  $H_2SO_4$  and  $HNO_3$  were employed during the washing steep
- Acidity, structure, and photocatalytic activity depend of the acid agent
- Lewis acid sites are formed with  $HCl$ , Brønsted acid sites are promoted by  $HNO_3$
- $HNO_3$  improves the photocatalytic activity of the nanotubes of  $TiO_2$

## Abstract

In this work, the acid and photocatalytic properties of titanate nanotubes (NTs) were surveyed. The surface acidity of the NTs was characterized by FTIR with lutidine and pyridine. The photocatalytic degradation of phenol in aqueous suspension was performed to test the photocatalytic properties of the NTs. The results were compared with those obtained from commercial  $TiO_2$ . NTs were prepared by hydrothermal treatment of  $TiO_2$  nanoparticles in a  $NaOH$  aqueous solution. During the

washing step, three different acid agents (HCl, H<sub>2</sub>SO<sub>4</sub>, and HNO<sub>3</sub>) were used. TiO<sub>2</sub> nanoparticles were synthesized previously by the sol-gel method. The photocatalytic materials were characterized by FTIR, XRD, XPS, S<sub>BET</sub>, UV-vis, and HRTEM.

It was found that the used acid agent significantly affected the amount and type of acid sites. Brønsted acid sites were favored by the use of HNO<sub>3</sub>. Lewis acid sites were promoted when HCl was employed during the washing step, which is in contrast with the results obtained using the other acids chosen in this work. Besides, the use of HCl promoted the H<sub>2</sub>Ti<sub>3</sub>O<sub>7</sub> phase. The acid phase H<sub>2</sub>Ti<sub>4</sub>O<sub>9</sub>·H<sub>2</sub>O was favored when HNO<sub>3</sub> was used and H<sub>2</sub>SO<sub>4</sub> formed the H<sub>2</sub>Ti<sub>2</sub>O<sub>4</sub>·(OH)<sub>2</sub> acid phase. The presence of Cl, S, and N species on the NTs was not found. Furthermore, Na<sup>+</sup> ions were completely removed from the surface of the NTs, which were exchanged by H<sup>+</sup> ions.

It was found, in general, that the three catalysts presented a relatively high photocatalytic activity to remove phenol. However, NTs washed with HNO<sub>3</sub> (NT-HNO<sub>3</sub>) displayed the best photocatalytic activity compared to the other NTs. After 200 min, NT-HNO<sub>3</sub> reached a phenol degradation yield close to 100%. Commercial TiO<sub>2</sub> presented a phenol degradation yield close to 60%. It could be concluded that the acid phase (H<sub>2</sub>Ti<sub>4</sub>O<sub>9</sub>·H<sub>2</sub>O) and concentration of Brønsted acid sites promoted the photocatalytic activity of NT-HNO<sub>3</sub>.

**Keywords:** Nanostructures; Heat treatment; Crystal structure; FTIR; Rietveld analysis; XPS.

## 1. Introduction

Titanium dioxide (TiO<sub>2</sub>) is one of the most extensively studied support overcoats in photocatalysis and heterogeneous catalysts [1,2]. The optical, electronic and redox properties, surface acidity, and

pollutant-decomposition capacity have made possible the application of TiO<sub>2</sub> in gas-sensing elements, electrode materials, as well as in the production and storage of energy [3–7]. Recently, new TiO<sub>2</sub> structures such as nanotubes, nanofibers, nanoribbons, nanorods and nanowires have emerged. These TiO<sub>2</sub> nanostructures feature physicochemical properties that are different from those displayed by the traditional TiO<sub>2</sub> phases (anatase, brookite and rutile) [8,9]. In fact, TiO<sub>2</sub> nanotubes have been widely used principally for their great surface area and tubular structure that increases the number of active sites [10,11].

TiO<sub>2</sub> nanotubes can be synthesized by using several methods. The surfactant directed method, alumina templating synthesis, microwave irradiation, electrochemical synthesis, sol–gel template method and hydrothermal method are the most employed [11-13]. However, the alkaline hydrothermal method is probably the most popular. The high reactivity, low energy requirement, relatively non-polluting set-up and simple aqueous solution control, represent the main advantages of this method [14].

The methodology involves the thermal treatment of TiO<sub>2</sub> with NaOH loaded into an autoclave. During the formation of TiO<sub>2</sub> nanotubes, in 1999, researchers introduced the washing step with an acid (HCl) with the purpose of removing the Na<sup>+</sup> ion to form Ti-OH bonds, followed by a washing process producing Ti-O--H-O-Ti [15-17]. The main structures formed after the washing step are the following acid phases H<sub>2</sub>Ti<sub>3</sub>O<sub>7</sub>, H<sub>2</sub>Ti<sub>2</sub>O<sub>5</sub>·H<sub>2</sub>O, H<sub>2</sub>Ti<sub>4</sub>O<sub>9</sub>, H<sub>2</sub>Ti<sub>4</sub>O<sub>9</sub>·H<sub>2</sub>O and H<sub>x</sub>Ti<sub>2-x/4</sub>O<sub>4-x/4</sub>·H<sub>2</sub>O. These kinds of structures are known as titanate nanotubes. However, the mechanism for the formation of titanate nanotubes is, up to now, controversial [1,18]. Recently, we reported [19] TiO<sub>2</sub> nanostructures such as nanotubes, nanofibers and nanowires featuring both Brönsted and Lewis acid sites. Hara et al. [20] showed that TiO<sub>2</sub> nanosheets exhibited an excellent catalytic performance for the Friedel–Crafts alkylation of toluene with benzyl chloride. In general,

it has been reported that the acid properties of the titanate nanotubes are different from those featured by the starting material, but how the surface acidity can be modified is not clear yet.

In this work, the effect of three different acids employed during the washing step upon structure, surface acidity and photocatalytic activity of the nanotubes is reported. How the surface is modified and the kind of acid sites that are favored in the NTs were also analyzed. It was found that the improved photocatalytic activity of the TiO<sub>2</sub> nanotubes is attributed to the modification of the physicochemical properties as well as the surface acidity.

## **2. Experimental**

### *2.1. Preparation of titanate nanotubes*

Titanate nanotubes were prepared by the hydrothermal method as reported elsewhere [21]. TiO<sub>2</sub> nanoparticles were prepared by the sol-gel method. 36.7 mL of titanium (IV) isopropoxide (Aldrich 97%) were dissolved in 145 mL of 2-propanol (Baker 99.9%) under constant stirring. To adjust the reaction medium at pH 1, HNO<sub>3</sub> was used. Bidistilled water was employed to accomplish the hydrolysis. The solution was maintained under stirring and reflux up to the gel formation. The gel was dried at 70°C for 12 h. Finally, the material was annealed at 350°C for 4 h.

For the synthesis of nanotubes, 3.0 g of TiO<sub>2</sub> obtained by the sol-gel method were dissolved in 60 mL of a NaOH aqueous solution (7N). The solution was mixed in a closed cylindrical Teflon-lined autoclave Parr reactor at 140 °C for 24 h, rotating the autoclave at 200 rpm. Thereafter, the solution was filtered with HCl, H<sub>2</sub>SO<sub>4</sub> and HNO<sub>3</sub> until reaching a pH close to 2. The solution was washed with abundant deionized water to reach a pH value of 7. Finally, the material was dried under vacuum at 80 °C for 12 h. The solid was annealed in air at 300 °C for 4 h. The samples were labeled as NT-HCl, NT-H<sub>2</sub>SO<sub>4</sub> and NT-HNO<sub>3</sub>, respectively.

### *2.2. Characterization*

X-ray diffraction (XRD) patterns of samples packed in a glass holder were recorded at room temperature with a Cu K $\alpha$ 1.2 source (1.5418 Å) on a Siemens D-500 diffractometer having a theta–theta configuration and a graphite secondary-beam monochromator. The data were collected for scattering angles ( $2\theta$ ) ranging from 4 to 80° with a 0.02° step for 1 s per point. High resolution transmission electron microscopy (HRTEM) analyses of the samples were performed in a JEOL 2200FS microscope operating at 200 kV and equipped with a Schottky-type field emission gun and an ultrahigh resolution pole piece ( $C_s = 0.5$  mm, point-to-point resolution, 0.190 nm). The samples were ground, suspended in isopropanol at room temperature and dispersed by ultrasonic stirring. Then, an aliquot of the solution was dropped on a 3-mm-diameter-lacey-carbon-copper grid.

Textural properties were determined on an ASAP-2000 analyzer from Micrometrics. The specific surface area ( $S_{BET}$ ) was calculated from the Brunauer–Emmett–Teller equation from N<sub>2</sub> physisorption at 77 K. The pore size distribution was obtained by the Barrett–Joyner–Halenda method from the desorption branch. A Thermo Scientific, Evolution 600, UV–vis spectrometer (UV-vis) was used to record directly the diffuse reflectance spectra between 200 and 800 nm, using the reflectance spectra as a reference at room temperature.

Pyridine and lutidine (2,6-dimethylpyridine) spectra were recorded on a Nicolet 8700 spectrophotometer with a 4 cm<sup>-1</sup> resolution, accumulating 50 scans. In the cell, all the samples were treated in vacuum at 400 °C for 1 h. Pyridine and lutidine were admitted and adsorbed. Evacuations were performed from room temperature up to 400 °C. The acidity per surface area for Lewis and Brønsted acid sites was calculated by following the pyridine method [22]. Rietveld refinement was performed with the Maud software, using the reported atomic position as a reference [23-24].

The suspension of titanate nanotubes was monitored with a Microtrac (Zetatrac) to quantify the zeta potential. The aqueous suspension was used as a function of the pH. Prior to the experiment,

the pH of the aqueous suspension was set to the desired value with the HCl or NaOH (0.01 M) solutions.

### 2.3. Photocatalytic activity.

The nanotubes were tested for the photocatalytic degradation of phenol (Fermont) using a Pyrex reactor at room temperature, which was irradiated directly with a UV-A lamp (365 nm) in the dark. For the photocatalytic tests, 200 mg of catalyst were used. The aqueous solution contained 20 ppm of phenol (0.1062 mol/L of phenol). A Pyrex reactor (250 mL), which was irradiated directly by a UV-A lamp (365 nm) in the dark, was used. The catalysts were exposed for 215 min to the UV-A light. The pH of the solution was maintained at a value of 7.

To quantify the photocatalytic degradation of phenol, a UV-vis evolution 600 equipment (Thermo Fisher Scientific) was employed. During the photoreaction, aliquots were collected at selected time intervals. Samples of 1 mL were extracted with a syringe. The sample was filtered through a 0.45 mm PTFE filter (Millipore). The photocatalytic degradation efficiency was calculated as follows:  $\eta(\%) = (C_i - C_t)/C_i * 100$ , where  $C_i$  is the initial concentration of phenol (mol/L) and  $C_t$  is the concentration of phenol after irradiation at a given time (mol/L). The filtered titanate nanotube samples were also analyzed using a Shimadzu Total Organic Carbon Analyzer (VCPN) with Non-Dispersive Infra-Red detector (NDIR) to determine the amount of Total Organic Carbon (TOC).

### 2.4. Phenol adsorption

Adsorption experiments were conducted at pH 7.0 using 200 mg of titanate nanotubes contained in a solution (200 mL) of 20 ppm of phenol (0.1062 mol/L of phenol). A Pyrex reactor (250 mL) was used for the adsorption experiments. The solutions were stirred at 300 rpm and 25°C. Aliquots were taken and centrifuged and then analyzed by UV-visible spectrophotometer to determine the phenol initial and equilibrium concentrations in the solutions. The amount of phenol adsorbed onto

the titanate nanotubes at equilibrium was calculated according to the following equation:  $q_e = (C_0 - C_e) \cdot V / M$ , where  $q_e$  is the equilibrium adsorption amount (mg/g),  $C_0$  is the phenol initial concentration (mg/L),  $C_e$  is the phenol equilibrium concentration (mg/L) from the absorption band intensity at 270 nm,  $V$  is the phenol solution volume (L) and  $M$  is the mass of the titanate nanotubes (g).

## Results and discussion

### 3.1. XRD

The XRD patterns for the NT samples annealed at 300°C are shown in Fig.1. The results confirm the presence of the different titanate acids ( $H_2Ti_3O_7$ ,  $H_2Ti_4O_9 \cdot H_2O$  and  $H_2Ti_2O_4 \cdot (OH)_2$ ) that were obtained by washing with HCl,  $H_2SO_4$  and  $HNO_3$ , respectively [25-26]. According to JCPDS, the different diffraction peaks matched the 36-0654, 36-0655 and 57-0123 cards. For the NT-HCl sample: (100) at 9.79°, (110) at 24.37°, (311) at 28.3° and (020) at 48.5°. For the NT- $H_2SO_4$  sample: (200) at 9.77°, (110) at 24.23°, (311) at 28.01° and (020) at 48.5°. For the NT- $HNO_3$  sample: (200) at 9.18°, (110) at 24.3°, (600) at 28.14° and (020) at 48.14° [28], respectively, see Fig. 1(A).

The XRD patterns of the NT- $H_2SO_4$  and NT-HCl samples show a little change in the peaks located at  $2\theta = 9.79^\circ$  and  $9.77^\circ$  with respect to the one of NT- $HNO_3$  located at  $2\theta = 9.18^\circ$ , which indicates that these titanate nanotubes are sensitive to the acid agent. This result is in good agreement with those obtained by some researchers [27-29] who have stated that the acid washing step exerts a significant effect on the titanate nanotubes in terms of elemental composition and annealing behavior. The phases for the NT-HCl, NT- $H_2SO_4$  and NT- $HNO_3$  samples annealed at 300°C were determined by the Rietveld method, using the atomic position of  $Na_2Ti_3O_7$  (JCPDS 720-148). It was found that the structure without  $H_2O$  is very similar to the space group 11, which is in good

agreement with Donk et al. [24]. In Fig. 1(B), a high proportion of the  $\text{H}_2\text{Ti}_2\text{O}_5\cdot\text{H}_2\text{O}$  phase with respect to the anatase phase can be observed for the NT-HCl, NT- $\text{H}_2\text{SO}_4$  and NT- $\text{HNO}_3$  samples. Table 1 also presents the phase composition of the nanotubes for several temperatures. Morgado et al. [30] reported a refinement at  $400^\circ\text{C}$  with a value of 51.8 % for the  $\text{TiO}_2(\text{B})$  phase and 48.2 % for the anatase phase. However, by using the Rietveld Method, the optimized lattice parameters in our XRD patterns were as follows:  $a= 8.11$   $b= 4.11$  and  $c= 9.77$  with an angle of  $100.11^\circ$ .

### 3.2. HRTEM morphology

The morphologies of NT-HCl, NT- $\text{H}_2\text{SO}_4$  and NT- $\text{HNO}_3$ , annealed at  $300^\circ\text{C}$ , were investigated by HRTEM. The micrographs are shown in Fig. 2. A high yield of multiwall titanate nanotubes with inner and outer diameters between 2 and 3 nm and 8 and 10 nm, respectively, can be observed in Fig. 2. The wall layers of the NT- $\text{H}_2\text{SO}_4$  and NT- $\text{HNO}_3$  samples are composed of two and four layers with an interlayer spacing between 0.75 and 0.85 nm from reflection  $d_{200}$ , respectively. The fast Fourier transform (FFT) for the NT-HCl sample revealed characteristic spots of titanate nanotubes which represent the (200) and (110) planes. The NT- $\text{H}_2\text{SO}_4$  sample featured an ordered tubular structure formed with the  $d_{200}$  and  $d_{110}$  planes. The inset in Fig. 2(B) shows a magnification, where titanate nanotubes are seen mainly, and unreacted particles of the starting material are not observed; this fact is consistent with what was found in the X-ray patterns.

NT- $\text{HNO}_3$ , reported in Fig. 2(C), showed a uniform morphology and an open-end-tubular structure with external and internal diameters between 8 and 2 nm, respectively. After annealing the materials at  $300^\circ\text{C}$ , it could be observed that the interlayer spacing between the nanotube walls was still conserved; these fringes have a space of 0.8 nm. This phenomenon is related to the dehydration of interlayer OH groups of the  $\text{H}_2\text{Ti}_2\text{O}_4\cdot(\text{OH})_2$  structure [28], which reduced the interlayer distance. The morphology variations of the titanate nanotubes were very similar to those featured by the NT-HCl and NT- $\text{HNO}_3$  samples. The NT- $\text{H}_2\text{SO}_4$  sample exhibits a different morphology, principally

inside the nanotubes with well aligned fringes of 0.75 nm, which correspond to the  $d_{200}$  plane of  $\text{H}_2\text{Ti}_4\text{O}_9 \cdot \text{H}_2\text{O}$  located at  $2\theta = 9.77^\circ$ , reported in Fig. 2(B).

### 3.3. Textural properties

The BET surface areas for the NT-HCl, NT-H<sub>2</sub>SO<sub>4</sub> and NT-HNO<sub>3</sub> samples annealed at 300 °C are shown in Table.1. In our case, the NT-H<sub>2</sub>SO<sub>4</sub> sample showed a high specific area (422 m<sup>2</sup>/g), while the NT-HCl and NT-HNO<sub>3</sub> samples showed a slight change in the  $S_{\text{BET}}$  values at around 375 to 369 m<sup>2</sup>/g, respectively. However, it has been reported [1,13,28] that the acid washing step is a critical parameter that modifies the surface area and pore volume. In fact, the acid washing step removes the electrostatic repulsion and promotes the formation of titanate nanotubes. Furthermore, the acid treatments replace Na<sup>+</sup> ions by H<sup>+</sup> ions. The variation of surface charge caused by ion exchange of Na<sup>+</sup> by H<sup>+</sup> ions leads to the scrolling of sheets into nanotubes, improving the physicochemical properties of the titanate nanotubes with respect to those exhibited by the starting material.

### 3.4. Surface acidity

The surface acidity of the materials synthesized in this work is presented in Fig. 4. Table 1 also presents the concentration of Brönsted and Lewis acid sites for several temperatures. The bands observed in Figs. 3(A), 3(B) and 3(C) at 1450 cm<sup>-1</sup> for the NT-HCl, NT-H<sub>2</sub>SO<sub>4</sub> and NT-HNO<sub>3</sub> samples are assigned to coordinated pyridine bound to Lewis acid sites [31]. The band located at 1540 cm<sup>-1</sup> is assigned to pyridinium ions formed by Brönsted acid sites [31]. This behavior was not observed for TiO<sub>2</sub> in its rutile, brookite and anatase phases; it was only observed for titanate nanotubes [32-33], which indicates that titanate nanotubes possess both Brönsted and Lewis acid sites whose concentration can be modified through the different acid washings [19-20].

The amounts of Brönsted and Lewis acid sites in NT-HCl, NT-H<sub>2</sub>SO<sub>4</sub> and NT-HNO<sub>3</sub> are quantified in Table 1. The three samples showed a remarkable behavior regarding the absorption on Brönsted

and Lewis acid sites. In fact, the intensity of the peak for Lewis acid sites was remarkably higher than that of Brönsted acid sites, principally for the NT-HCl and NT-H<sub>2</sub>SO<sub>4</sub> samples. The NT-HNO<sub>3</sub> sample showed a predominance of Brönsted acid sites from room temperature up to 400°C. At high temperatures, from 200 to 400°C, the intensities of pyridine adsorption decreased on both Brönsted and Lewis acid sites. In the NT-H<sub>2</sub>SO<sub>4</sub> sample, the bands of the Brönsted and Lewis acid sites disappear at 400°C. For the NT-HCl sample, the Lewis acid sites remained up to 400°C, as reported in Figs. 3(A) and 3(B).

In summary, three samples with different behavior patterns and different quantities of Brönsted and Lewis acid sites in the 100-400°C range were obtained. This effect is particularly important because titanate nanotubes can also be used in catalytic or photocatalytic reactions and not just, because of their high surface areas, as supports of dispersed metals. In this sense, the surface acidity plays an important role. As for the NT-HCl, NT-H<sub>2</sub>SO<sub>4</sub> and NT-HNO<sub>3</sub> samples, they can be employed at low and middle temperatures since they show thermal stability until 420°C. In this sense, we reported [34] the catalytic activity of NT supports for the NO reduction with NH<sub>3</sub>, obtaining a conversion of 52% of NO at 420°C. The NT samples showed different amounts of Brönsted acid sites owing to the scrolling of the Ti-O-H bonds.

In Fig. 3(D), it can be observed that pyridine is coordinated in different kinds of sites, depending of the type of structure. In our case, at 200°C, H<sub>2</sub>Ti<sub>3</sub>O<sub>7</sub> for NT-HCl, H<sub>2</sub>Ti<sub>4</sub>O<sub>9</sub>·H<sub>2</sub>O for NT-H<sub>2</sub>SO<sub>4</sub> and H<sub>2</sub>Ti<sub>2</sub>O<sub>4</sub>·(OH)<sub>2</sub> for NT-HNO<sub>3</sub> were deconvoluted between 1660 and 1680 cm<sup>-1</sup> and normalized to sample weight, where the main absorption peak appeared at 1590 cm<sup>-1</sup>, solely in the NT-HCl and NT-H<sub>2</sub>SO<sub>4</sub> samples, corresponding to the 8a ring vibration mode of a H-bonded pyridine [35-36]. Likewise, in the NT-HCl, NT-H<sub>2</sub>SO<sub>4</sub> and NT-HNO<sub>3</sub> samples, the main peak appears at 1603 cm<sup>-1</sup>, suggesting that pyridine is coordinated to Lewis acid sites mainly in NT-HCl, which is in contrast to NT-H<sub>2</sub>SO<sub>4</sub> and NT-HNO<sub>3</sub>.

### 3.5. Lutidine adsorption

Lutidine (2,6-dimethylpyridine) is considered as a more sensitive molecule for characterizing Brönsted acid sites. This study was carried out to uphold the results obtained by using pyridine, and, in addition, the O-H groups that can be formed on the surface of the titanate nanotubes by employing different acid agents such as HCl, H<sub>2</sub>SO<sub>4</sub> and HNO<sub>3</sub> in the washing step. It has been reported [19,37] that titanate nanotubes possess a high number of OH groups when the starting material featured the anatase phase. Fig. 5(A) shows the FTIR spectra of Lutidine adsorbed on the NT-HCl, NT-H<sub>2</sub>SO<sub>4</sub> and NT-HNO<sub>3</sub> samples. The analysis was carried out at 200°C and normalized to sample weight. The bands located at 1642 and 1625 cm<sup>-1</sup> for the three samples are characteristic of Lutidine adsorbed on Brönsted acid sites [38].

For the NT-HCl sample, a strong band located at 1580 cm<sup>-1</sup> is observed. This band is assigned to the vibrating 8b mode of an H-bonding with its corresponding 8a vibrating mode of the peak at 1602 cm<sup>-1</sup>. These bands are less intense in the NT-H<sub>2</sub>SO<sub>4</sub> and NT-HNO<sub>3</sub> samples. Another band is located between 1592 and 1594 cm<sup>-1</sup>, which is attributed to the 8a mode of physisorbed lutidine molecules with their corresponding 8b mode overlapping the 8b mode of H-bonding lutidine located at 1580 cm<sup>-1</sup>, Fig. 5(B) [39]. This result supports the one obtained by pyridine FTIR, showing a strong H-bonding band in NT-HCl in comparison to NT-H<sub>2</sub>SO<sub>4</sub> and NT-HNO<sub>3</sub>. This fact suggests that the NT-HCl sample tends to interact more with Lewis acid sites than the NT-HNO<sub>3</sub> sample, which interacts with Brönsted acid sites. This statement was confirmed by absorption of pyridine and lutidine. It can be then conclude that the kind of acid agent can accelerate the washing process, playing an important role in the atomic arrangement of the Ti-O---H titanate nanotubes.

### 3.6. XPS characterization

The XPS scan is shown in Fig. 6. In the inset shown in Fig. 6(A), the 0-450 eV interval can be observed, which is where the S 2p (176-160 eV), Cl 2p (185-210 eV) and N 1s (394-406 eV) signals appeared. The Cl, S and N signals are not found due to the fact that these compounds were eliminated during the washing process. Besides, these species do not affect the type of acid sites; they only modify the atomic arrangement of the titanate nanotubes during the washing step.

The survey of the NT-HCl, NT-H<sub>2</sub>SO<sub>4</sub> and NT-HNO<sub>3</sub> samples displays signals originated from O 1s, Ti 2p<sub>1/2</sub> and Ti 2p<sub>3/2</sub>, which are easily identified at binding energies around 531, 464 and 458 eV, respectively. The features observed at 1224, 1108, 1075 and 979 eV correspond to the Auger peaks of C, N, Ti and O. It is important to note that signals related to Na, Mg and Ca are not detected because they were eliminated during the washing process. Figs. 6(B) and (C) show the O 1s and Ti 2p photoelectron peaks.

The deconvolution of O1s displays three peaks [40]. The first peak is assigned to oxygen in the crystal lattice at 530 eV [40]. The second peak is correlated with surface hydroxyl groups OH<sup>-</sup> at 531 eV [40]. The third peak is related to physical water adsorbed at 532 eV [40]. The three peaks are reported in Fig. 6(B). The content of OH<sup>-</sup> groups was observed in this order: NT-HNO<sub>3</sub> > NT-H<sub>2</sub>SO<sub>4</sub> > NT-HCl. In these sense, OH<sup>-</sup> groups are very useful because they contribute to the supply of active oxygen species and provide active sites during the photocatalytic degradation of phenol. Ti 2p displays two peaks at around 464 and 458 eV, which correspond to Ti<sup>4+</sup> 2p<sub>1/2</sub> and 2p<sub>3/2</sub>. This information supports the fact that titanate nanotubes mainly present the oxidation state Ti<sup>4+</sup> [41]. The NT-HCl, NT-H<sub>2</sub>SO<sub>4</sub> and NT-HNO<sub>3</sub> samples maintain a constant separation of 5.7 eV. However, the shift shown in Fig. 6(C) is attributed to the interaction between the titanium and oxygen atoms [42].

### 3.7. UV-vis

The optical properties of the NT samples annealed at 300°C are generally related to their nanostructure, where the electronic state, defect state and energy level structure are important parameters [43]. Fig. 7 shows the UV–vis spectra for P25, NT-HCl, NT-H<sub>2</sub>SO<sub>4</sub> and NT-HNO<sub>3</sub>. The calculated band gaps (E<sub>g</sub>) for the different NT samples are also shown in Fig.7. The band gap (E<sub>g</sub>) for the samples obtained employing HCl, H<sub>2</sub>SO<sub>4</sub> and HNO<sub>3</sub> during the washing step varies over a narrow interval of 3.18 and 3.34 eV. In comparison with the TiO<sub>2</sub> anatase phase that displays a band gap of 3.2 eV [44], the absorption edge of NT-HNO<sub>3</sub> and NT-HCl is shifted to the UV-vis light region.

The increase in the band gap of the TiO<sub>2</sub> nanotubes is attributed to the quantization of electronic states and the dimensionality reduction from 3D to 2D and/or 1D [45]. Besides, the variations in the band gaps for NT-HCl, NT-H<sub>2</sub>SO<sub>4</sub> and NT-HNO<sub>3</sub> are caused by the acid washing step, which modifies the absorption due to changes regarding the structure, phase composition and morphology. The band gap of the NTs prepared with H<sub>2</sub>SO<sub>4</sub> exhibited a value of 3.18 eV; the nanotubes with HNO<sub>3</sub> increased the band gap sharply to 3.34 eV and the nanotubes with HCl showed a band gap of 3.28 eV.

### *3.8. Zeta potential*

The changes in the titanate nanotubes employing different acid agents during the washing step were followed by measuring the Z-potential of their aqueous suspension as a function of the pH. The results are reported in Fig. 8. The NT-HCl, NT-H<sub>2</sub>SO<sub>4</sub> and NT-HNO<sub>3</sub> samples showed an isoelectric point (IEP) at pH 7 for NT-HCl, at pH 7.2 for NT-HNO<sub>3</sub> and 6 for NT-H<sub>2</sub>SO<sub>4</sub>, respectively. The Z-potential curve reached negative values below -60 mV at pH values above 7.5, reaching a maximum value for NT-HCl of -35 mV. The Z-potential values of the three NT-HCl, NT-H<sub>2</sub>SO<sub>4</sub> and NT-HNO<sub>3</sub> samples were significantly different.

The measured Z-potential for the anatase phase has been reported with a value of 5.1 to 5.4 [46-47]. For Degussa P25, the reported values range from 5.7 to 6.0 [46-47]. In our case, our samples display slightly higher values than those reported in the literature [46-47]. Besides, it is possible that the values of Z-potential are sensitive to the kind of structure. For instance, this study showed the formation of layered titanate phases ( $\text{H}_2\text{Ti}_3\text{O}_7$ ,  $\text{H}_2\text{Ti}_4\text{O}_9 \cdot \text{H}_2\text{O}$  and  $\text{H}_2\text{Ti}_2\text{O}_4 \cdot (\text{OH})_2$ ). The use of  $\text{HNO}_3$  led to the formation of Brönsted acid sites, displaying an isoelectric point (IEP) at pH 7.2. In the case of HCl, Lewis acid sites were formed and the IEP was reached at pH 7.

### 3.9. Photocatalytic activity

Fig. 9(A) displays the photocatalytic degradation of phenol as a function of the UV light irradiation time over the P25, NT-HCl, NT- $\text{H}_2\text{SO}_4$  and NT- $\text{HNO}_3$  samples. The photocatalytic degradation of phenol is an apparent first-order reaction verified by the linear transform  $-\ln C_0/C = f(t)$  illustrated in Fig. 9(E). Fig. 9(B) displays the UV-vis spectral change of 20 ppm of phenol as a function of the irradiation time during the photocatalytic activity of the NT- $\text{H}_2\text{SO}_4$  photocatalysts. It was found, Fig. 9(A), that phenol with an initial concentration of 20 mg/L was removed by 96% after irradiation and 215 min for NT- $\text{H}_2\text{SO}_4$ . The photocatalytic removal rates of phenol by Degussa P-25, NT-HCl and NT- $\text{HNO}_3$  were 65, 92 and 94%, respectively.

The photocatalytic activity of the nanostructured materials was found to be dependent on the  $\text{H}_2\text{Ti}_3\text{O}_7$  phase, composition, annealing temperature, surface area and acid properties. In fact, the acid washing step is a critical process that modifies the surface area, pore volume, structure, phase composition and morphology, and band gap, as well as the acid properties, which improve the photocatalytic degradation of phenol with respect to the  $\text{TiO}_2$  anatase and rutile phases.

The surface areas and acid properties are the key factors that influence both the activity of the photocatalysts and the efficiency of the photocatalytic reactions. The synergetic effect of a larger surface area and the presence of Brönsted and Lewis acid sites shown by the scrolling structure of

the NT-HCl, NT-H<sub>2</sub>SO<sub>4</sub> and NT-HNO<sub>3</sub> samples play a major role in having a higher photocatalytic activity degradation of phenol.

Properties such as crystalline phase (H<sub>2</sub>Ti<sub>3</sub>O<sub>7</sub>, H<sub>2</sub>Ti<sub>4</sub>O<sub>9</sub>•H<sub>2</sub>O and H<sub>2</sub>Ti<sub>2</sub>O<sub>4</sub>•(OH)<sub>2</sub>), morphology, surface area and acidity type (Brönsted and Lewis) present in these TiO<sub>2</sub> nanostructures make them very profitable supports for potential applications in environmental pollution control. The equilibrium adsorption of the nanostructured materials used in this work is reported in Fig. 9(C). The equilibrium adsorption was reached after 1 h. Our results reported in Fig. 9(C) show that phenol was weakly adsorbed on the titanate nanotubes. After 60 min, the adsorption of phenol reached the equilibrium. The adsorption capacity is 2.1 mg of phenol per g of nanotubes for NT-H<sub>2</sub>SO<sub>4</sub>, 1.98 mg/g for HCl, 1.71 mg/g for NT-HNO<sub>3</sub>, and 1 mg/g for commercial P-25.

The photocatalytic mineralization of phenol was conducted for the NT-HCl, NT-H<sub>2</sub>SO<sub>4</sub> and NT-HNO<sub>3</sub> samples in order to determine and verify the efficiency in removing phenol and total organic carbon (TOC). The TOC results are reported in Fig. 9(D). It can be observed, in Fig. 9(D), that the best sample to remove phenol and carry on until complete mineralization was NT-HNO<sub>3</sub> followed by NT-H<sub>2</sub>SO<sub>4</sub> and NT-HCl. Besides, it was found by the total organic carbon analysis that close to 80% of phenol was degraded to CO<sub>2</sub> and 20% of phenol formed other intermediate compounds on NT-HNO<sub>3</sub>. The CO<sub>2</sub> formation by degradation of phenol was close to 70% for NT-H<sub>2</sub>SO<sub>4</sub> and around 65% for HCl.

It has been reported [48] that the photocatalytic degradation of phenol follows a pseudo first-order kinetic reaction. In this sense, the rate constant was obtained for our materials. The results are reported in Fig. 9(E) and Table 2. Eq. (1) was used to obtain the rate constant. However, Eq. (1) has been developed for a homogeneous reaction based on Eq. (2).

$$tk = -\ln \frac{C_A}{C_{A_0}} \quad (1)$$

$$\frac{dN_A}{dt} = r_A V \quad (2)$$

Eq. (2) does not consider the catalyst mass. The correct form to obtain the rate constant is the following Eq. (3):

$$\frac{dN_A}{dt} = r_A W \quad (3)$$

where  $W$  is the mass of catalyst employed during the reaction. Separating and integrating Eq. (3) we obtain:

$$tkW \frac{C_{A0}}{N_{A0}} = -\ln\left(\frac{C_A}{C_{A0}}\right) \quad (4)$$

where  $N_{A0}$  represents the amount of phenol (mol),  $C_{A0}$  is the phenol initial concentration (mol/L),  $W$  is the weight of catalyst ( $g_{cat}$ ),  $X_A$  is the conversion of phenol (%),  $t$  is the time (min),  $k$  is the rate constant (mol/L $g_{cat}$ -s). Eq. (4) represents the best approach to obtain the rate constant for the photocatalytic system reported in this work, instead of Eq. (1). In this case, the rate constant can be compared for each material considering the weight of catalyst. The slope  $m$  of the straight line reported in Fig. 9(E) gives the rate constant. The highest rate constant for photocatalytic degradation of phenol was obtained for the NT-HNO<sub>3</sub>.

## Conclusions

The effect of using different acid washing agents such as HCl, H<sub>2</sub>SO<sub>4</sub> and HNO<sub>3</sub> upon titanate nanotubes was analyzed. A high concentration of Lewis acid sites in the sample washed with HCl was found. The sample washed with HNO<sub>3</sub> showed a remarkable concentration of Brönsted acid sites. The sample washed with H<sub>2</sub>SO<sub>4</sub> displayed the generation of both acid sites at low temperature. The surface acidity of the nanotubes was confirmed by adsorption of pyridine and lutidine.

In summary, titanate nanotubes can produce effective Lewis and Brönsted sites by only modifying the acid washing agent, treating them until 300 °C. Besides, the results show that the acid washing

agent modifies the structure of the titanate nanotubes to form  $\text{H}_2\text{Ti}_3\text{O}_7$  (with  $\text{HCl}$ ),  $\text{H}_2\text{Ti}_4\text{O}_9 \cdot \text{H}_2\text{O}$  (with  $\text{H}_2\text{SO}_4$ ) and  $\text{H}_2\text{Ti}_2\text{O}_4 \cdot (\text{OH})_2$  (with  $\text{HNO}_3$ ). In this sense, NTs interact differently with the kind of acid agent, generating Brönsted and Lewis acid sites, which makes NTs very attractive as supports for a great number of photocatalytic applications.

## **Acknowledgments**

The authors want to thank the financial support provided by the project D.00477 from the Mexican Institute of Petroleum. R. Camposeco acknowledges the support provided by CONACyT and LINAN-IPICYT.

## References

- [1] H. H. Ou, S. L. Lo, *Separation and Purification Technology*. 58 (2007) 179–191.
- [2] M. Breyse, P. Afanasiev, C. Geantet, M. Vrinat. *Catal. Today*. 86 (2003) 5–16.
- [3] P. Panagiotopoulou, A. Christodoulakis, D. I. Kondarides, S. Boghosian. *J. Catal.* 240 (2006) 114–125.
- [4] Q. Zhao, M. Li, J. Chu, T. Jiang, H. Yin. *App. Surf. Sci.* 255 (2009) 3773– 3778.
- [5] G. F. Ortiz, I. Hanzu, T. Djenizian, P. Lavela, J. L. Tirado, P. Knauth. *Chem. Mat*, 21 (2009) 63–67.
- [6] D. V. Bavykin, J. M. Friedrich, F. C. Walsh, *Advanced Materials*. 18 (2006) 2807–2824.
- [7] U. Diebold, *Surf. Sci. Rep.* 48 (2003) 53-229.
- [8] A.V. Grigorieva, E. A. Goodilin, K. L. Dubova, et al. *Solid State Sciences*. 12 (2010) 1024–1028.
- [9] Z.V. Saponjic, N.M. Dimitrijevic, D.M. Tiede, A.J. Goshe, X. Zuo, L.X.Chen, A.S. Barnard, P. Zapol, L. Curtiss, T. Rajh, *Adv. Mater.* 17 (2005) 965–971.
- [10] K. Okada, Y. Takamatsu, Y. Tokudome, A. Nakahira, M. Takahashi, *J. Sol–Gel Sci. Technol.* 65 (2013) 36–40.
- [11] C. C. Tsai, J. N. Nian, H. Teng. *App. Surf. Sci.* 253 (2006) 1898–1902.
- [12] L. L. Costa, A.G. Prado. *Photochem. Photobiol A*. 201 (2009) 45-49.
- [13] V.E. Nawin, S. Noriaki, C. Tawatchai, K. Takeyuki, T. Wiwut. *Nanotechnol.* 19 (2008) 1-6.
- [14] C. K. Lee, C.C. Wang, M. D. Lyu, L. C. Juang, S. S. Liu, S. H. Hung. *Colloid Interface Sci.* 316 (2007) 562-569.

- [15] T. Kasuga, M. Hiramatsu, A. Hoson, T. Sekino, K. Niihara. *Adv. Mater.* 11 (1999) 1307-1311.
- [16] X. B. Chen, S. S Mao. *Chem. Rev.* 107 (2007) 2891-2959.
- [17] Q. Chen, W. Z. Zhou, G. H. Du, L. M. Peng. *Adv. Mater.* 14 (2002) 1208-1211.
- [18] Á. Kukovecz, M. Hodos, E. Horváth, G. Radnóczy, Z. Kónya, I. Kiricsi, J. Phys.Chem. B 109 (2005) 17781–17783.
- [19] R. Camposeco, S. Castillo, I. Mejia-Centeno, J. Navarrete, R. Gómez. *Materials Characterization.* 90 (2014) 113–120.
- [20] M. Kitano, E. Wada, K. Nakajima, S. Hayashi, S. Miyazaki, H. Kobayashi, M. Hara. *Chem. Mater.* 25 (2013) 385–393.
- [21] R. Camposeco, S. Castillo, I. Mejia, V. Mugica, R. Carrera, A. Montoya, M. Morán Pineda, J. Navarrete, R. Gómez, *J. Catal. Commun.* 17 (2012) 81–88.
- [22] E. Selli, L. Forni. *Microporous Mesoporous Mater.* 31 (1999) 129–140.
- [23] Maud, materials analysis using diffraction by L. Lutterotti, version <http://www.ing.unitn.it/lutero/maud> (revised on January 20, 2017).
- [24] D. H. Kim, J. S. Jang, S. S. Han, K. S Lee, S. H. Choi, A. Umar, J. W. Lee, et al. *J. Phys. Chem. C* 113 (2009) 14034–14039.
- [25] R. Ma, Y. Bando, T. Sasaki, *Chemical Physics Letters*, 380 (2003) 577–582.
- [26] A. Thorne, A. Kruth, D. Tunstall, J. T. Irvine, W.J. Zhou. *Phys. Chem. B.* 109 (2005) 5439-5444.
- [27] A.L. Papa, N. Millot, L. Salvot, R. Chassagnon, O. J. Helntz. *Phys. Chem. C.* 113 (2009) 12682-12689.
- [28] J. Yang, Z. Jin, X. Wang, W. Li, J. Zhang, S. Zhang, X. Guo, Z. Zhang. *Dalton Trans.* (2003) 3898–3901.

- [29] T. Bezrodna, G. Puchkovska, V. Shimanovska, I. Chashechnikova, T. Khalyavka. *J. Appl. Surf. Sci.* 2003, 214, 222–231.
- [30] E. Morgado Jr, M. A. Abreu, O. R. Pravia, B. A. Marinkovic, P. M. Jardim, F. C. Rizzo, A. S. Araújo. *Solid State Sciences* .8 (2006) 888–900
- [31] G. Busca, *Chem. Rev.* 107 (2007) 5366–5410.
- [32] Y. Zarifyanc, V. Kiselev, A. S. Petrov, R.V. Prudnikov, S.V. Khrustaleva, G. D. Chukin, *Kinet. Katal.* 15 (1974) 1091–1096.
- [33] J. Araña, A. Peña Alonso, J. M. Doña Rodríguez, G. Colón, J.A. Navío, J. Pérez Peña, *Appl. Catal. B.* 89 (2009) 204–213.
- [34] R. Camposeco, S. Castillo, V. Mugica, I. Mejía-Centeno, J. Marín, *Chem Eng. J.* 242 (2014) 313–320.
- [35] D. Cook, *Canad. J. Chem.* 39 (1961) 2009–2024.
- [36] G. Ertl, H. Knözinger, J. Weitkamp, *Handbook of Heterogenous Catalysis*, VCH Verlagsgesellschaft mbH, Germany, (1997).
- [37] Z. Zheng, J. Teo, X. Chen, H. Liu, Y. Yuan, E. R. Waclawik, Z. Zhong, H. Zhu. *Chem. Eur. J.* 16 (2010) 1202–1211.
- [38] A. Corma, C. Rodellas, V. J. Fornes. *J. Catal.* 88 (1984) 374–381.
- [39] C. Morterra, G. Cerrato, G. Meligrana. *Langmuir*, 17 (2001) 7053–7060.
- [40] R. Sanjinés, H. Tang, H. Berger, F. Gozzo, G. Margaritondo, *J. Appl. Phys.* 75 (1994) 2945–2951.
- [41] B. K. Kaleji, R. Sarraf-Mamoory, *Mater. Res. Bull.* 47 (2012) 362–369.
- [42] J. Jiang, Q. Gao, Z. Chen, *Journal of Molecular Catalysis A: Chemical* 280 (2008) 233–239.
- [43] L.D. Zhang, C.M. Mo, *Nanostruct. Mater.* 6 (1995) 831–834.

- [44] H. Tang, F. Levy, H. Berger, P. E. Schmid, *Phys. Rev. B* 52 (1995) 7771-7774.
- [45] R. Ma, Y. Bando, T. Sasaki, *J. Phys. Chem. B* 108 (2004) 2115–2119.
- [46] R. Sprycha, *J. Colloid Interface Sci.* 110 (1986) 278–281.
- [47] J. Gustafsson, P. Mikkola, M. Jokinen, J.B. Rosenholm, *Colloids Surf. A* 175 (2000) 349–359.
- [48] B. Koubaissy, J. Toufaily, M. El Murr, T.J. Daou, H. Hafez, G. Joly, P. Magnoux, T. Hamieh, *Cent. Eur. J. Eng.* 2(3) (2012) 435-444.

## List of Figures

**Fig. 1.** (A) XRD patterns for NT-HCl, NT-H<sub>2</sub>SO<sub>4</sub> and NT-HNO<sub>3</sub> and the standard (JCPDS 36-0654, 36-0655, 57-0123 and 047-0124) diffraction patterns for H<sub>2</sub>Ti<sub>3</sub>O<sub>7</sub>, H<sub>2</sub>Ti<sub>4</sub>O<sub>9</sub>·H<sub>2</sub>O, H<sub>2</sub>Ti<sub>2</sub>O<sub>4</sub>·(OH)<sub>2</sub> and H<sub>2</sub>Ti<sub>2</sub>O<sub>5</sub>·H<sub>2</sub>O. (B) Rietveld refinement plots for NT-HCl, NT-H<sub>2</sub>SO<sub>4</sub> and NT-HNO<sub>3</sub>, the upper marks correspond to H<sub>2</sub>Ti<sub>2</sub>O<sub>5</sub>·H<sub>2</sub>O and the lower marks correspond to the anatase phase.

**Fig. 2.** HR-TEM for the titanate nanotubes: (A) NT-HCl, (B) NT-H<sub>2</sub>SO<sub>4</sub> and (C) NT-HNO<sub>3</sub> annealed at 300°C with diffraction planes corresponding to H<sub>2</sub>Ti<sub>3</sub>O<sub>7</sub>, H<sub>2</sub>Ti<sub>4</sub>O<sub>9</sub>·H<sub>2</sub>O and H<sub>2</sub>Ti<sub>2</sub>O<sub>4</sub>·(OH)<sub>2</sub>.

**Fig. 3.** Pyridine adsorption FTIR spectra of titanate nanotubes: (A) NT-HCl, (B) NT-H<sub>2</sub>SO<sub>4</sub> and (C) NT-HNO<sub>3</sub> in the 1400-1700 cm<sup>-1</sup> region. Pyridine was evacuated from room temperature (RT) to 400°C. (D) Pyridine adsorption for the 8a ring vibrating mode in the 1580-1660 cm<sup>-1</sup> region for the NT-HCl, NT-H<sub>2</sub>SO<sub>4</sub> and NT-HNO<sub>3</sub> samples, corresponding to bonded-H weakly interacting with pyridine evacuated at 200°C.

**Fig. 4.** Concentration of Brönsted (A) and Lewis acid sites (B) at 100, 200, 300 and 400 °C on the surface of the NT-HCl, NT-H<sub>2</sub>SO<sub>4</sub> and NT-HNO<sub>3</sub> samples.

**Fig. 5.** (A) Lutidine adsorption FTIR spectra for the HCl, H<sub>2</sub>SO<sub>4</sub> and HNO<sub>3</sub> samples. (B) Lutidine adsorption (8a and 8b ring vibrating mode regions) FTIR for the NT-HCl, NT-H<sub>2</sub>SO<sub>4</sub> and NT-HNO<sub>3</sub> samples annealed at 300°C and evacuated at 200°C.

**Fig. 6.** (A) XPS spectra for the hydrothermally treated NT-HCl, NT-H<sub>2</sub>SO<sub>4</sub> and NT-HNO<sub>3</sub> samples, (B) O1s and (C) Ti 2p cores.

**Fig. 7.** UV-vis for the titanate nanotubes NT-HCl, NT-H<sub>2</sub>SO<sub>4</sub> and NT-HNO<sub>3</sub> annealed at 300°C and Degussa P25.

**Fig. 8.** Z-potential profiles for NT-HCl, NT-H<sub>2</sub>SO<sub>4</sub> and NT-HNO<sub>3</sub> samples (employed different acid agents) as a function of pH in water.

**Figure. 9.** (A) Conversion of phenol at pH 7 for NT-HCl, NT-H<sub>2</sub>SO<sub>4</sub> and NT-HNO<sub>3</sub> annealed at 300°C. (B) UV-vis spectra of phenol obtained for NT-H<sub>2</sub>SO<sub>4</sub> photocatalysts. (C) Equilibrium absorption for NT-HCl, NT-H<sub>2</sub>SO<sub>4</sub> and NT-HNO<sub>3</sub>. (D) TOC removal for NT-HCl, NT-H<sub>2</sub>SO<sub>4</sub> and NT-HNO<sub>3</sub>, and (E) rate constant for NT-HCl, NT-H<sub>2</sub>SO<sub>4</sub> and NT-HNO<sub>3</sub> photocatalysts.

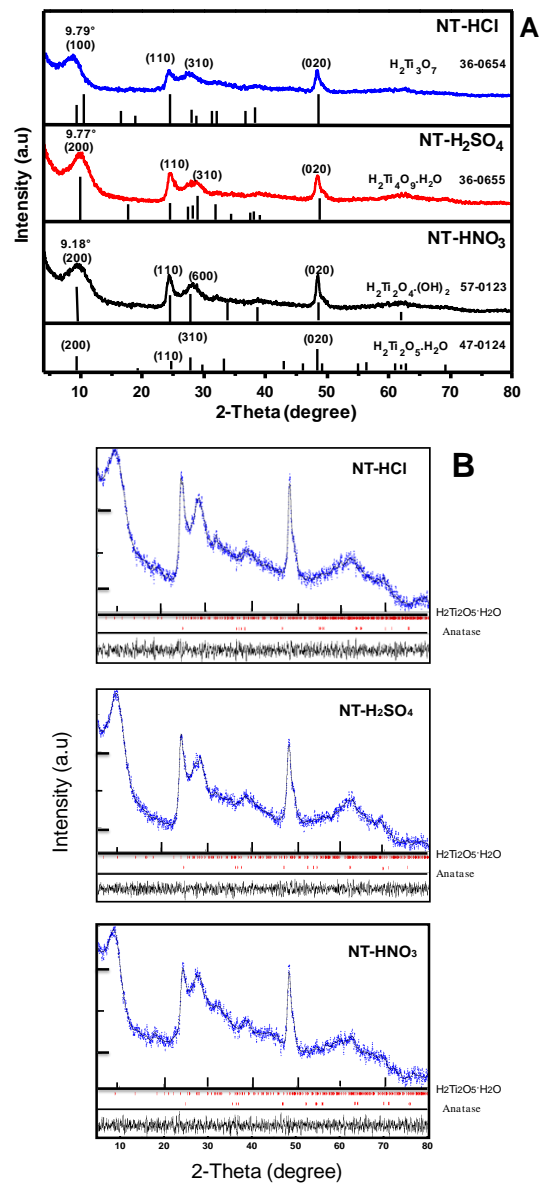


Fig. 1

R. Camposeco et al.

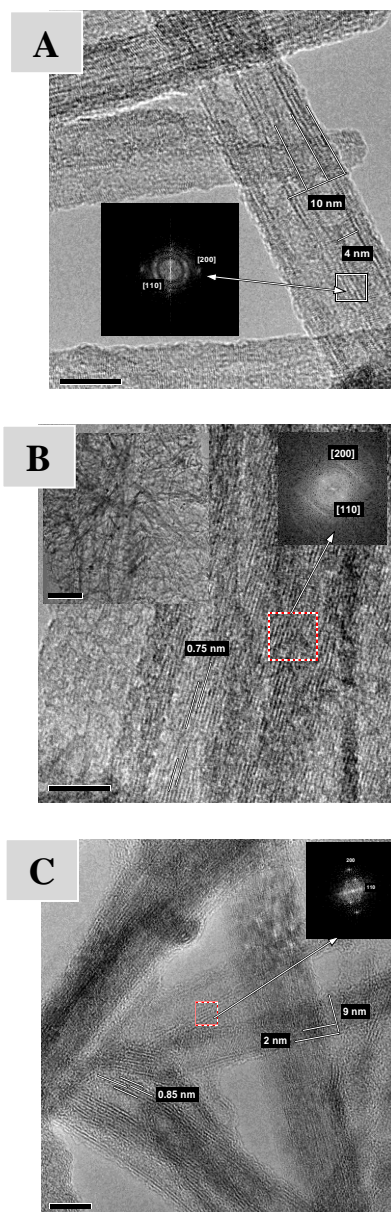


Fig. 2  
R. Camposeco et al.

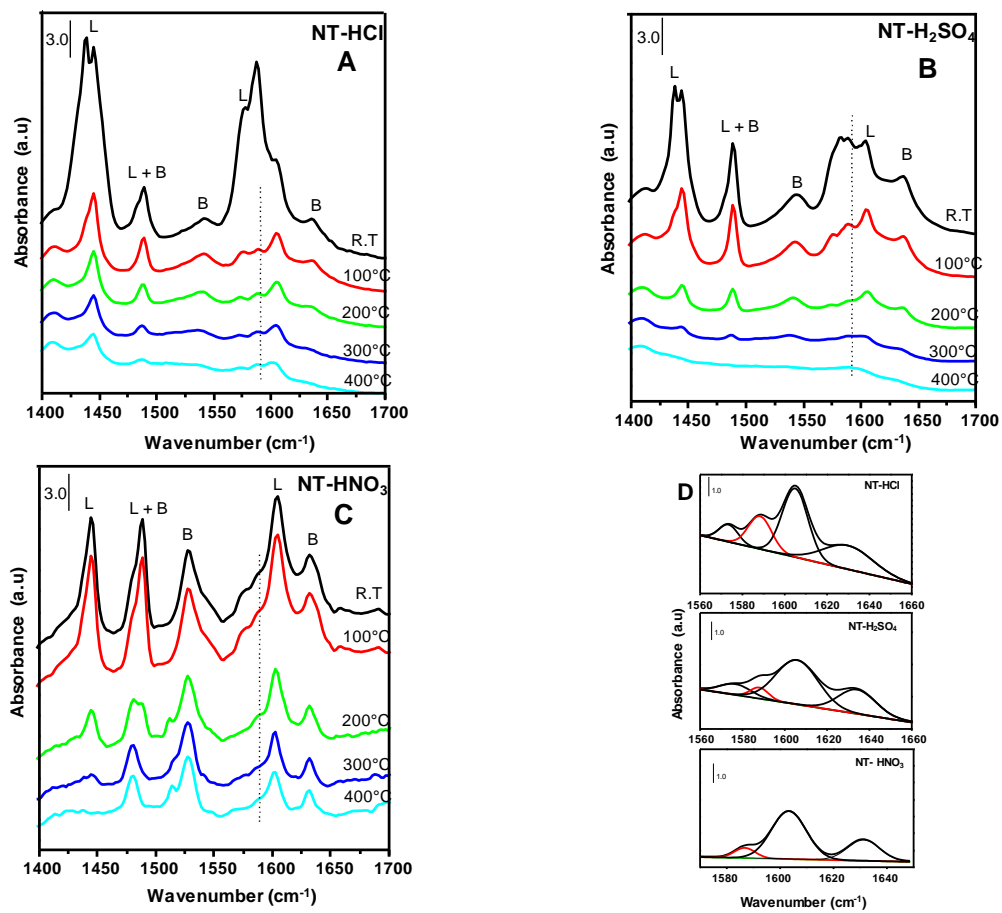


Fig. 3  
R. Camposeco et al.

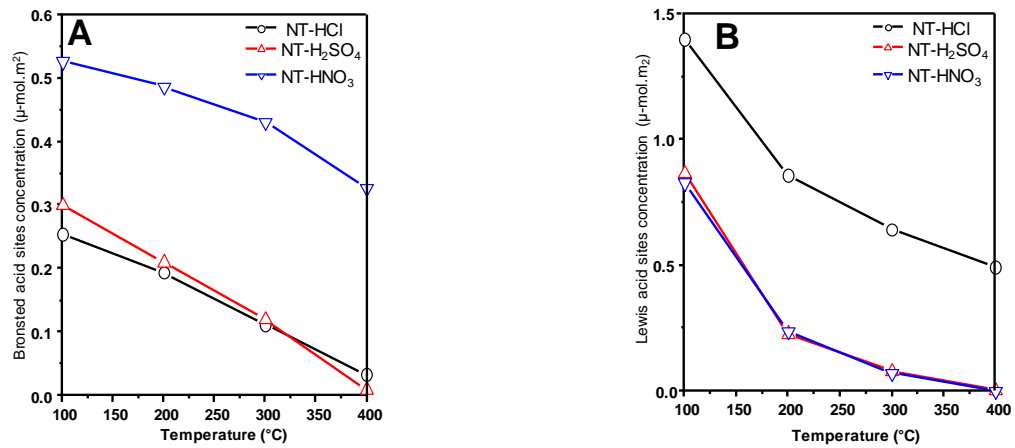


Fig. 4  
R. Camposeco et al.

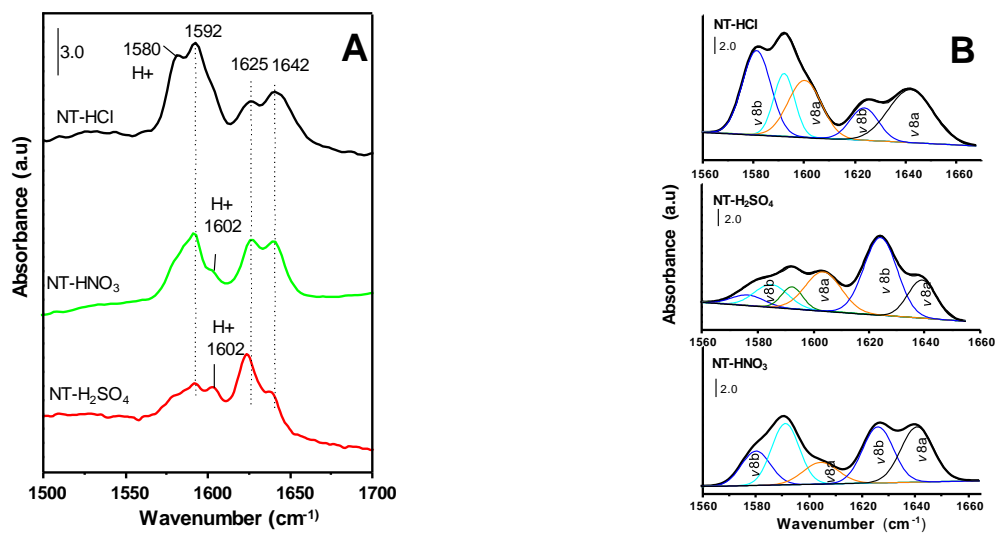


Fig. 5  
R. Camposeco et al.

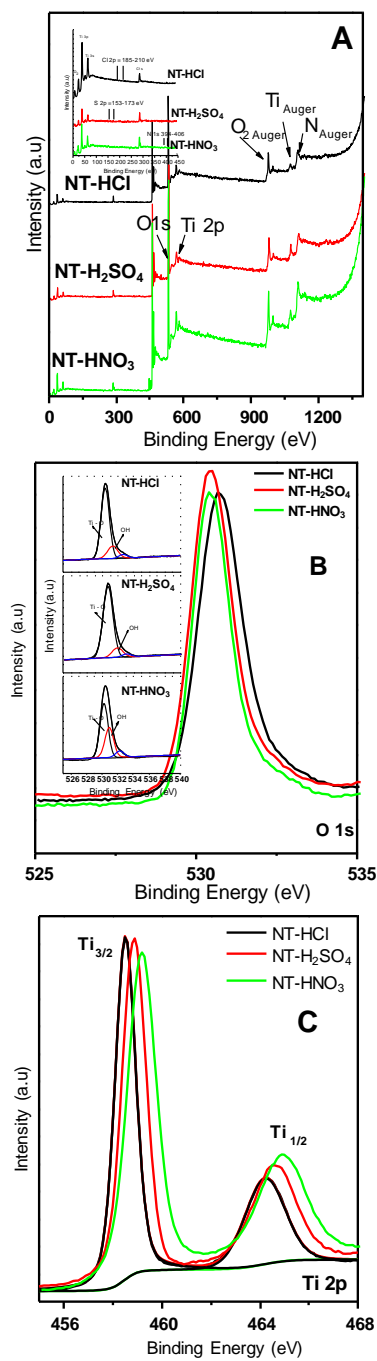


Fig. 6  
R. Camposco et al.

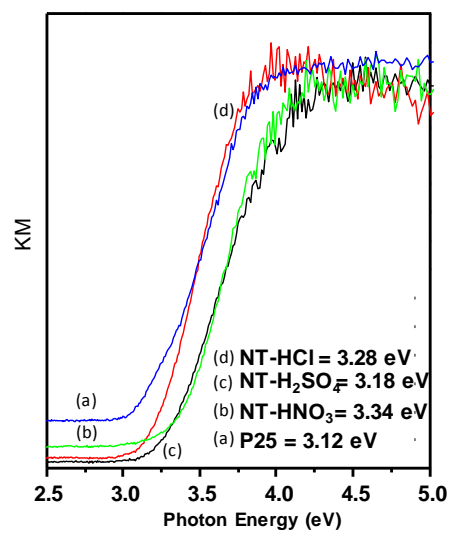


Fig. 7  
R. Camoseco et al.

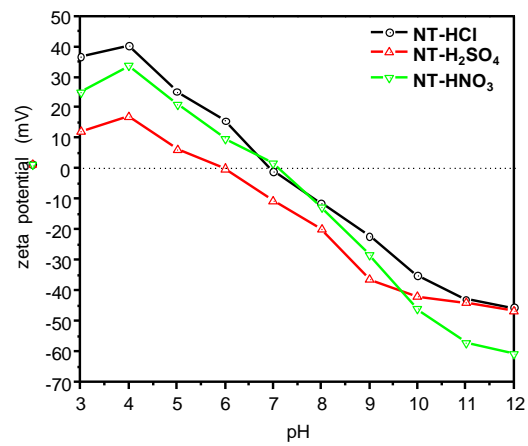


Fig. 8  
R. Camposeco et al.

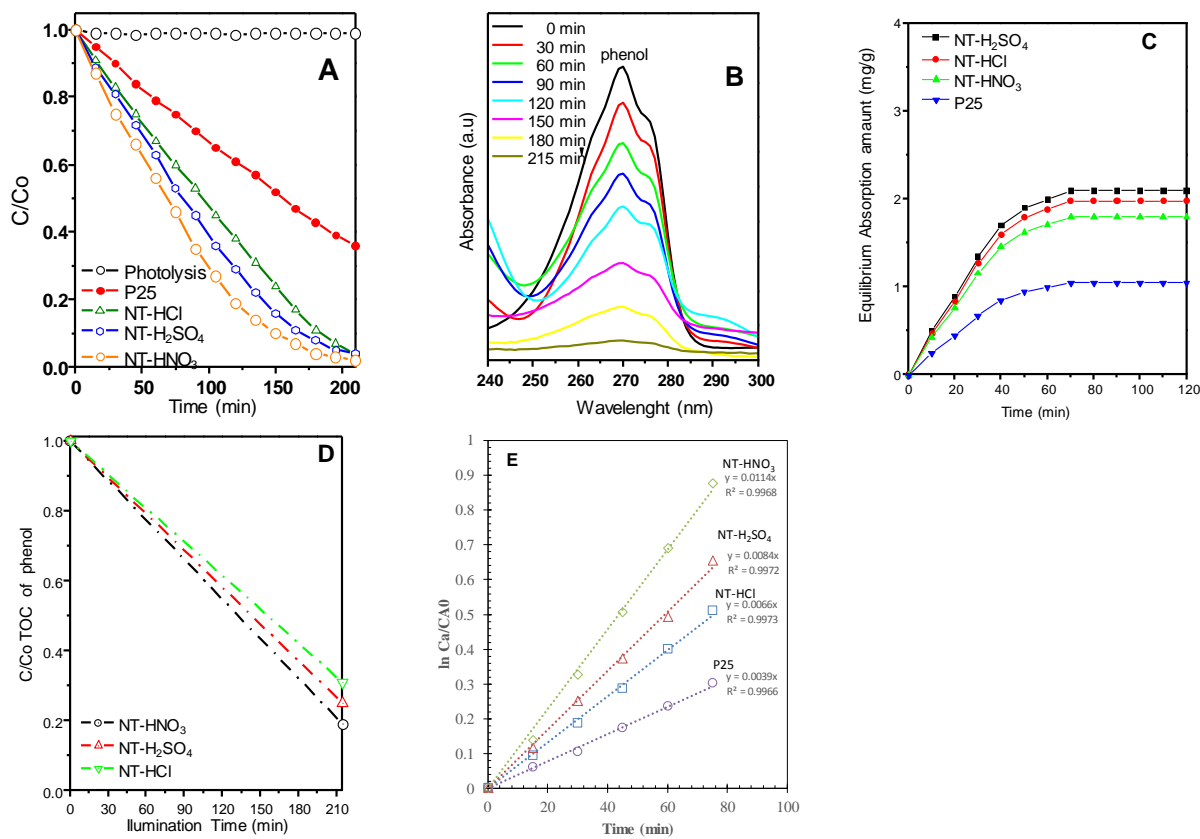


Fig. 9  
R. Camposeco et al.

## Tables

**Table 1.** BET surface areas for the titanate nanotubes and surface acid sites per BET area for the NT samples at 100, 200, 300 and 400°C.

Sample	S <sub>bet</sub> (m <sup>2</sup> /g)	D <sub>p</sub> (Å)	V <sub>p</sub> (cm <sup>3</sup> /g)	NaOH (N)	C <sub>Lewis</sub> (μ-mol.m <sup>-2</sup> )	C <sub>Brönsted</sub> (μ-mol.m <sup>-2</sup> )	C <sub>Total</sub> (μ-mol.m <sup>-2</sup> )	Temperature (°C)	Composition (%)
NT/HCl	375	145	1.33	7	1.39 0.85 0.64 0.49	0.25 0.19 0.11 0.03	1.65 1.05 0.75 0.52	100°C 200°C 300°C 400°C	Anatase= 16 H <sub>2</sub> Ti <sub>2</sub> O <sub>5</sub> •H <sub>2</sub> O =84
NT/H <sub>2</sub> SO <sub>4</sub>	422	141	1.49	7	0.85 0.22 0.07 0.00	0.29 0.21 0.12 0.009	1.14 0.43 0.19 0.01	100°C 200°C 300°C 400°C	Anatase= 18 H <sub>2</sub> Ti <sub>2</sub> O <sub>5</sub> •H <sub>2</sub> O =82
NT/HNO <sub>3</sub>	369	149	1.37	7	0.82 0.23 0.07 0.00	0.52 0.48 0.43 0.32	1.35 0.72 0.50 0.32	100°C 200°C 300°C 400°C	Anatase= 23 H <sub>2</sub> Ti <sub>2</sub> O <sub>5</sub> •H <sub>2</sub> O =77
P25	52	56	0.34	....	1.13 0.97 0.42 0.10	... ... ... ...	1.13 0.97 0.42 0.10	100°C 200°C 300°C 400°C	Anatase= 70 Rutile= 30

Table 1.  
R. Camposeco et al

**Table 2.** Rate constant for the photocatalytic activity of phenol for NT-HCl, NT-H<sub>2</sub>SO<sub>4</sub>, NT-HNO<sub>3</sub> and P-25.

Material	k (from eq. 1) 1/s	k (from eq. 4) L/g <sub>cat</sub> -s
NT-HNO <sub>3</sub>	0.0114	1.140x10 <sup>-5</sup>
NT-H <sub>2</sub> SO <sub>4</sub>	0.0084	0.084x10 <sup>-5</sup>
NT-HCl	0.0066	0.066x10 <sup>-5</sup>
P25	0.0039	0.039x10 <sup>-5</sup>

Table 2.  
R. Camposeco et al.